This is a pre-print version of the following article: D. Ruijters, B. M. ter Haar Romeny, P. Suetens: "Vesselness-based 2D-3D registration of the coronary arteries", International Journal of Computer Assisted Radiology and Surgery 4(4): 391-397, June 2009, doi:10.1007/s11548-009-0316-z. The final publication is available at springerlink.com.

Vesselness-based 2D - 3D Registration of the Coronary Arteries

Daniel Ruijters

Philips Healthcare,
Cardio/Vascular Innovation,
Veenpluis 6, 5680DA Best, the Netherlands
danny.ruijters@philips.com

Bart M. ter Haar Romeny

Technische Universiteit Eindhoven,
Biomedical Engineering, Image Analysis and Interpretation,
Eindhoven, the Netherlands

Paul Suetens

Katholieke Universiteit Leuven,
Medical Image Computing,
ESAT/Radiologie, Universitair Ziekenhuis Gasthuisberg,
Leuven, Belgium

Purpose: Robust and accurate automated co-registration of the coronary arteries in 3D CTA and 2D X-ray angiography during percutaneous coronary interventions (PCI), in order to present a fused visualization.

Methods: A novel vesselness-based similarity measure was developed, that avoids an explicit segmentation of the X-ray image. A stochastic optimizer searches the optimal registration using the similarity measure.

Results: Both simulated data and clinical data were used to investigate the accuracy and capture range of the proposed method. The experiments show that the proposed method outperforms the iterative closest point method in terms of accuracy (average residual error of 0.42 mm versus 1.44 mm) and capture range (average 71.1 mm / 20.3° versus 14.1 mm / 5.2°).

Conclusion: The proposed method has proven to be accurate and the capture range is ample for usage in PCI. Especially the absence of an explicit segmentation of the interventionally acquired X-ray images considerably aids the robustness of the method.

Percutaneous Coronary Interventions, Chronic Total Occlusions, X-ray fluoroscopy - CT image fusion, Registration

Introduction

Coronary artery disease (CAD) is one of the most common pathologies in the industrialized world. In catheter-based percutaneous coronary interventions (PCI) the impaired blood flow is restored by placing a stent in the narrowed vessel segment. The navigation of the catheter is especially challenging for chronic total occlusions, since the vessel tree distal to the occlusion is not visible in the X-ray images. A fused presentation of the X-ray image sequence and pre-processed computed tomographic angiography (CTA) data containing the occluded vessel segment, can be very useful during the guidance and treatment of the diseased vasculature. Furthermore such a fused visualization can also aid in increased accurate stent placement for any PCI, using pre-annotated CTA data, *e.g.* indicating plaque locations.

Such a fused visualization requires the 2D X-ray data and the 3D CTA data to be co-registered. 2D-3D image registration has a number of clinical applications, such as radiotherapy planning and verification [1-4], surgery planning and guidance [4-7], and minimal invasive vascular treatment in coronary artery [8], peripheral [6, 9, 10] and neuro-interventions [11-14].

Most algorithms for 2D-3D image registration can be classified as either intensity-based or feature-based. Intensity-based methods [4-6, 10, 12] directly use the pixel and voxel values to calculate a similarity measure, and require no or little segmentation. Feature-based methods [2, 7, 11, 13-16] are based on a segmentation of landmark features in the images. Once this segmentation has been obtained, the registration step can be performed quite fast. The segmentation, however, is not always trivial or robust, and erroneous segmentations can lead to erroneous registrations.

Due to their tubular structure, vessels occupy a relatively small fraction of the image, which especially poses a hurdle in intensity-based image registration. Therefore feature-based registration has received particular interest for vascular 2D-3D registration. Many feature-based methods are based on the Iterative Closest Point (ICP) approach [17], which relies on minimizing the sum of minimal distances between the feature points in the reference and projected image. Fitzgibbon [18] has shown that the Distance Transform can be used in ICP-like registration, in order to improve its efficiency. This approach has been applied [13, 14] to register the neuro-vasculature by segmenting the vessel tree in the 2D and the 3D image.

Methods and materials

The objective of a 2D-3D registration algorithm is to find a spatial mapping between the 2D and the 3D image. Typically a registration algorithm consists of a similarity measure, indicating the quality of a given spatial mapping, and an optimization algorithm, which iteratively searches the optimum of the similarity measure. The search space consists of the multi-dimensional control variables of the spatial mapping.

Projection

A common part in 2D-3D registration algorithms is the projection of a point in 3D space on the X-ray detector plane. In our case the 3D coronary vessel tree is projected on the detector plane. In order to perform this projection, a 4x4 matrix M is defined, such that $p = M \cdot v$, whereby p and v are homogenous coordinates. Vector v is then a coordinate in the 3D CTA space, and vector p a coordinate on the detector grid (the z value of p is simply disregarded).

Understanding the projection in mathematical detail is best accomplished by considering the components of the transformation chain separately. Matrix M can be decomposed into four matrices: $M = P \cdot T \cdot R \cdot O$, whereby P is the perspective transformation defined by the position of the focal spot (f_x, f_y, f_z), the position of the center of the detector (c_x, c_y, c_z), and the detector dimensions (d_x, d_y), as is illustrated in Figure 1.

$$P = \begin{pmatrix} 2/d_x & 0 & 0 & 2(f_x - c_x)/d_x \\ 0 & 2/d_y & 0 & 2(f_y - c_y)/d_y \\ 0 & 0 & 1 & 0 \\ 0 & 0 & 0 & 1 \end{pmatrix}$$

Matrix *T* is the rigid registration matrix, containing a rotation and a translation, which is manipulated during the optimization process. It should be noted that we do not perform a calibration of the X-ray equipment to correct for deviations of parameters delivered by the system, since these deviations are found to be smaller than the deformations that occur due to the cardiac and respiratory motion. Furthermore we rely on the registration process to correct also for the system inaccuracies.

Matrix *R* describes the viewing incidence of the X-ray C-arm geometry, and is determined by the L-arm (R_z), the propeller (R_y) and the roll rotation (R_x) of the C-arm, and can be expressed as $R = R_x \cdot R_y \cdot R_z$, (Figure 2). Note that the order of the matrix multiplications is given by the mechanics of the C-arm system.

Matrix *O* expresses the transformation from the frame of reference of the CTA dataset to the iso-centric X-ray coordinate frame. The rotational part of this matrix is extracted from the patient orientation information in the DICOM header of the CTA data. The translational part is established such that the center of the coronary vessel model in the CTA dataset corresponds to the iso-centric origin of the X-ray coordinate frame.

Similarity measure

In order to obtain a 3D model of the coronary vessels, they are segmented in the pre-operative 3D CTA datasets. There are good algorithms available for this task (*e.g.* [19]), and since it can be performed pre-operatively, it is not necessary to exclude manual interaction. A reliable and robust segmentation of the 2D X-ray angiography images can be more challenging, because of the projective nature of these images. Further, due to the intra-operative acquisition of the X-ray images, manual interaction or correction is not desirable. To overcome these limitations, we introduce a method which does not require an explicit segmentation of the 2D X-ray image.

We perform a Distance Transform (DT) on the projected 3D model in each iteration of the optimization process. The fact that the DT is calculated in every

iteration differs from DT-based ICP, where the points of the 3D model are projected on a static DT of the segmented 2D image. The Distance Transform computes for each pixel position *i* the distance to the nearest feature point *q* in a set of feature points *Ω*, which is the set of projected 3D points in our case (Figure 3a):

$$DT(i) = \min_{q \in \Omega} \| q - i \|$$

To achieve a rapidly declining distance weighting function D that yields only a high response close to the feature points, the squared DT is subtracted from a constant value *c* (Figure 3b):

$$D(i) = \max\left(0, \quad c - DT(i)^2\right)$$

A vesselness filter is applied to the 2D X-ray image (Figure 4a). The vesselness *V* expresses the likelihood that a particular pixel can be contributed to a vessel structure (Figure 4b). As such it can be regarded as a fuzzy segmentation. We apply a multi-scale vesselness filter, as proposed by Frangi [20] (note, however, that our similarity measure is not restricted to this particular vesselness filter). Our similarity measure can then be expressed as the sum of the product of the distance weighting function *D* and the vesselness *V* over all pixels in the image:

$$S = \sum_{i \in I} D(i) \cdot V(i)$$

Optimization strategy

The search space, consisting of the multi-dimensional control variables of the spatial mapping, is determined by three degrees of translational and three degrees of rotational freedom (rigid registration). The process of projecting 3D data on a 2D plane implies a considerable reduction of information. As a result there are many incorrect transformations that yield a relatively good similarity measure (*e.g.* projecting not corresponding vessel branches on each other), and form a local optimum in the search space.

We have used two optimization strategies; A standard Powell optimizer was chosen [21]. This method searches the parameter space by performing a line search in every direction of an orthonormal basis in each iteration. The basis can be adapted between the iterations.

The other strategy is an especially for this purpose developed stochastic optimization approach. The advantage of this method is the fact that it is less likely to get stuck in a local optimum. It uses a population of samples in the search space. In every iteration of the optimization algorithm the *n* best samples are taken, and they each create *m* new samples. The *m* 'children' of a sample are randomly generated according to a Gaussian normal distribution around the parent value for each variable in the parameter space. The standard deviation σ of the normal distributed random samples is multiplied with a reduction factor *r* for each iteration, since we assume that the global optimum is closer as we progress.
The initial σ can differ for each dimension of the search space. In our case we use a significantly smaller σ for the three rotation variables than for the three translation variables, since we can already perform a quite good estimation of the rotation of the 3D model, based on the DICOM information of the CTA data, and the viewing incidence of the X-ray C-arm system.

Results

We evaluated the presented similarity measure with respect to accuracy and capture range, comparing it against ICP-based registration. For the optimization strategy, we compared the standard Powell optimizer against the stochastic optimization strategy described in the previous section.
The accuracy and capture range was assessed, using simulated data. In order to perform this assessment, the coronary arteries were segmented from a real cardiac CTA data set, as well as the heart mask. From this CTA dataset a Digitally Reconstructed Radiograph (DRR) was constructed, which simulates an X-ray projection of the CTA data. In angiographic X-ray images the contrast medium is injected intra-vascularly, while the cardiac CTA images are obtained with intravenously administered contrast medium. To obtain a DRR from the CTA data that resembles an angiographic X-ray image, different X-ray attenuation coefficients assigned to the different segments, as is shown in Figure 5. The registration process is then started with a given offset translation and rotation. The advantage of the simulated data is the fact that the ground truth is known, and thus the error of the registration process can be quantified, see table 1.
Using the simulated data, on average a capture range of 14.1 mm translation and 5.2° rotation was established for the ICP-Powell combination, whereby the

capture range was defined as the set of initial translations and rotations with respect to the ground truth that still yielded a successful registration. The vesselness-Powell combination delivered a capture range of 43.8 mm and 22.1° respectively, and the vesselness-stochastic combination reached 71.1 mm and 20.3°. The average calculation time for the ICP method was only 82 ms, while vesselness-Powell combination took 2.7 seconds and the vesselness-stochastic combination calculated for 11.0 seconds. In order to obtain these figures 563 randomly initialized registrations were performed, 359 succeeded in finding the optimum within a margin of 3 mm and 3°, and 204 failed.

We further investigated the capture range using clinical data from four pairs of 2D X-ray images and 3D coronary vessel trees, segmented from cardiac CTA data. It should be mentioned that it is impossible to define an objective ground truth for such real world data, especially since the cardiac phase might differ somewhat for the 2D and 3D images of the pair. Therefore we proceeded in the following way: A large number (about 30 per dataset pair) of registrations were started from different starting positions (translation and rotation). The resulting transformation was then labeled either as 'successful' or 'erroneous' by an expert. The largest successful registration in sense of translated distance and rotated angle was taken as a measure for the capture range, see table 2.

The parameters of the stochastic optimizer during all measurements were set to perform 12 iterations with 25 samples each, whereby the 5 samples delivering the best results produced the `children' for the next iteration. The standard deviations σ of the normal distributed random samples were initialized on 12 mm for the translations and 4° for the rotations, and were multiplied with a reduction factor $r = 0.8$ between every iteration.

Discussion

The feature-based registration of a 3D vessel model, obtained from a CT, MR or 3DRA dataset to vascular X-ray images in non-cardiac applications is usually being performed using digital subtraction angiography (DSA) X-ray, since the vessel tree can be easily segmented in such DSA images. For the coronary arteries, however, cardiac and respiratory motion render DSA to be unavailable. Using traditional feature-based registration on unsubtracted X-ray images requires the explicit binary segmentation of the vasculature in the X-ray data. This

segmentation proved to be the weakest link in the 2D-3D registration, causing the registration to fail in many cases.

In the approach described in this article an explicit segmentation is avoided by directly using the vesselness image in our similarity measure. Furthermore, the squared distance transform guarantees that only vessel structures proximate to the projected centerlines contribute to the similarity measure, while it is wide enough to maintain a large capture range. We have demonstrated that the proposed vesselness-based similarity measure outperforms the Iterative Closest Point (ICP) method, both in sense of capture range and reliability.

We have shown that the stochastic optimization approach enlarges the capture range, since it is not likely to get stuck in a local optimum far from the global optimum. Future work might include evaluating other stochastic global optimization strategies, as e.g. proposed by Kennedy and Eberhart [22].

Figure 6 shows an example of a fused visualization of the cardiac CTA data and the X-ray fluoroscopy image. Once the registration has been established, the X-ray images can be fused with the CTA data in real-time. Since we performed the registration using a single static cardiac CTA phase, the coronary arteries in the X-ray sequence display a periodic motion around the coronary vessels, segmented from the CTA dataset. Though the ultimate goal would be to use 4D CTA data, while syncing the cardiac phases of the CTA and the X-ray data, the static 3D CTA already provides a good reference during the PCI treatment. The real-time X-ray image stream shows the advancement of the catheter, and the fused visualization aids in a more accurate placement of intra-vascular devices, such as stents.

Conclusion

When we started our search for a 2D-3D registration approach for the coronary arteries, we quickly abandoned intensity-based methods, because of their limited capture range for registration of vessel structures (intensity-based methods work best when there are large overlapping landmark areas, which is not a property of the vasculature). After initially disappointing results with feature-based registration, using a binary segmentation of the vessels in the 2D image, we developed a novel feature-driven 2D-3D registration method. This method is based on the iterative stochastic optimization of our similarity measure, which

relies on the 3D coronary vessel model, obtained from a cardiac CTA dataset, and a 2D X-ray image of the coronary arteries. The similarity measure is obtained by applying a vesselness filter to the 2D image, and then weighting it with a function based on the squared distance transform of the projected 3D vasculature. Our test results show that it performs very well for the task of 2D-3D registering of the coronary vessel tree.

In future work we intend to accelerate the calculation of the distance transform, since it forms the main bottleneck. Possibly, the graphics processing unit (GPU) could be used for this task. The multi-scale vesselness filter, which is rather expensive to calculate, only needs to be obtained once for the entire registration process, and therefore does not pose a significant bottleneck.

References

1. Gilhuijs KGA, van de Ven PJH, van Herk M. (1996) Automatic three-dimensional inspection of patient setup in radiation therapy using portal images, simulator images, and computed tomography data. Medical Physics 23:389-399
2. Murphy MJ (1997) An automatic six-degree-of-freedom image registration algorithm for image-guided frameless stereotaxic radiosurgery. Medical Physics 24:857-866
3. Clippe S, Sarrut D, Malet C, Miguet S, Ginestet C, Carrie C (2003) Patient setup error measurement using 3-D intensity-based image registration techniques. Int. J. Radiat. Oncol. Biol. Phys. 56(1):259-265
4. Markelj P, Tomaževič D, Pernuš F, Likar B (2008) Robust 3-D/2-D registration of CT and MR to X-ray images based on gradient reconstruction. Int J CARS 3:477-483
5. Lemieux L, Jagoe R, Fish DR, Kitchen ND, Thomas DGT (1994) A patient-to-computed-tomography image registration based on digitally reconstructed radiographs. Medical Physics 21:1749-1760
6. Weese J, Penney GP, Desmedt P, Buzug TM, Hill DLG, Hawkes DJ (1997) Voxel-based 2-D/3-D registration of fluoroscopy images and CT scans for image-guided surgery. IEEE Trans. Inf. Technol. Biomed. 1(4):284-293
7. Guéziec, A., Kazanzides, P., Williamson, B., Taylor, R.H.: Anatomy-based registration of CT-scan and intraoperative X-ray images for guidance of a surgical robot. IEEE Trans. Med. Imag. 17(5) (1998) 715-728
8. Turgeon GA, Lehmann G, Guiraudon G, Drangova M, Holdsworth D, Peters T (2005) 2D-3D registration of coronary angiograms for cardiac planning and guidance. Medical Physics 32(12):3737-3749
9. Breeuwer M., et al. (1998) The easi project-improving the effectiveness and quality of image-guided surgery. IEEE Transactions on Information Technology in Biomedicine 2(3):156-168

10. Penney GP, Batchelor PG, Hill DLG, Hawkes DJ, Weese J (2001) Validation of a two- to three-dimensional registration algorithm for aligning preoperative CT images and intraoperative fluoroscopy images. Medical Physics 28(6):1024-1032
11. Kita Y, Wilson DL, Noble JA (1998) Real-time registration of 3D cerebral vessels to X-ray angiograms. In: MICCAI '98:1125-1133
12. Hipwell JH, Penney GP, McLaughlin RA, Rhode K, Summers P, Cox TC, Byrne JV, Noble JA, Hawkes DJ (2003) Intensity-based 2-D-3-D registration of cerebral angiograms. IEEE Trans. Med. Imag. 22(11):1417-1426
13. Florin C, Williams J, Khamene A, Paragios N (2005) Registration of 3D angiographic and X-ray images using sequential monte carlo sampling. Computer Vision for Biomedical Image Applications 3765:427-436
14. Sundar H, Khamene A, Xu C, Sauer F, Davatzikos C (2006) A novel 2D-3D registration algorithm for aligning fluoroscopic images with pre-operative 3D images. In: SPIE Medical Imaging.
15. Feldmar J, Ayache N, Betting F (1997) 3D-2D projective registration of free-form curves and surfaces. Computer Vis. Underst. 65:403-424
16. Hamadeh A, Lavallée S, Cinquin P (1998) Automated 3-dimensional computed tomography and fluoroscopic image registration. Comput. Aided Surg. 3:11-19
17. Besl PJ, McKay ND (1992) A method for registration of 3-D shapes. IEEE Trans. Pattern Analysis and Machine Intelligence 14(2):239-256
18. Fitzgibbon AW (2001) Robust registration of 2D and 3D point sets. In: Proc. British Machine Vision Conference BMVC. Volume II. 411-420
19. Olabarriaga SD, Breeuwer M, Niessen WJ (2003) Minimum cost path algorithm for coronary artery central axis tracking in CT images. In: MICCAI '03:687-694
20. Frangi AF, Niessen WJ, Vincken KL, Viergever MA (1998) Multiscale vessel enhancement filtering. In: MICCAI'98:130-137
21. Press WH, Teukolsky SA, Vetterling WT, and Flannery BP (1992) Numerical Recipes in C: The Art of Scientific Computing. Cambridge University Press, New York, NY, USA.
22. Kennedy J, Eberhart RC (1995) Particle swarm optimization. In: Proc. IEEE Int. Conf. Neural Networks. Volume 4. 1942-1948

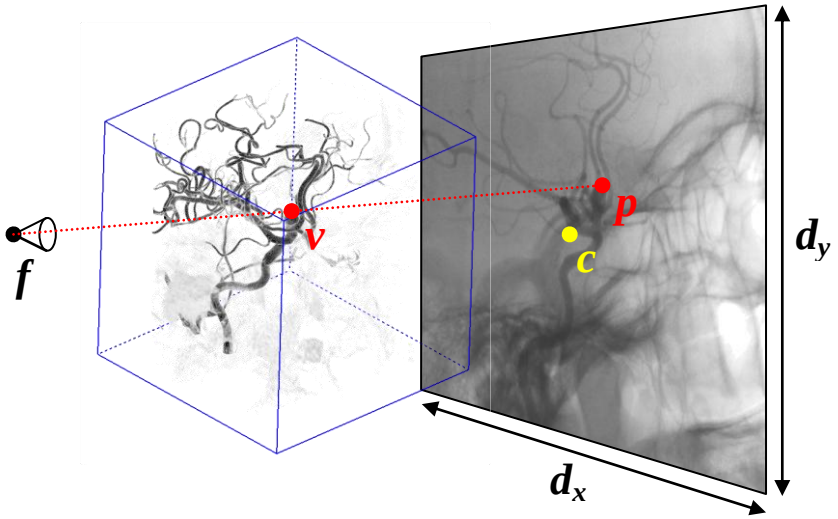

Fig. 1. The projection of a point in 3D space on the detector grid is determined by the position *f* of the focal spot and the position and orientation of the detector. The center of the detector is indicated by *c*, the detector dimensions by d_x and d_y, *v* is an arbitrary point in 3D space, and *p* represents its projection on the detector.

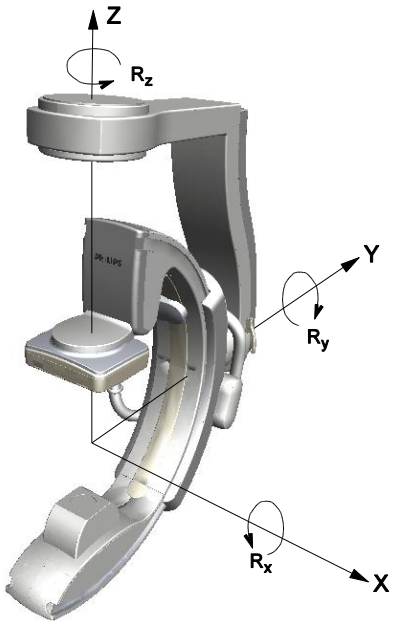

Fig. 2. The X-ray angiography C-arm system's geometry, and its degrees of freedom. The C-arm can be rotated around the x-axis by rolling in its sleeve (roll movement), around the y-axis (propeller movement) and z-axis (L-arm rotation).

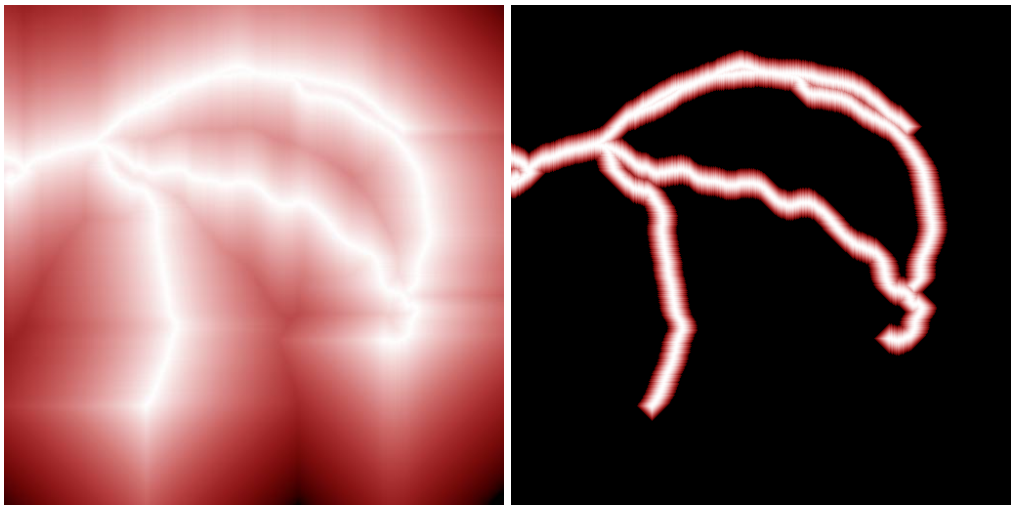

(a) (b)

Fig. 3. (a) Distance transform; The central axis of the segmented coronary vessels in the 3D CTA dataset is projected on the virtual detector plane. The distance transform of the projected points is depicted here, whereby lower intensities correspond to larger distances. (b) In order to have a function that declines more rapidly, the distance transform is squared.

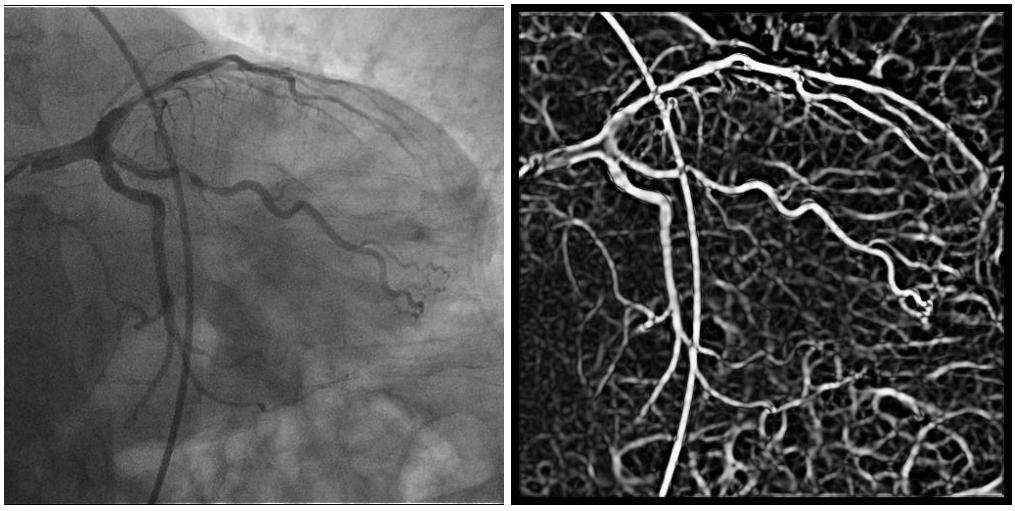

(a) (b)

Fig. 4. (a) X-ray image of the coronary arteries. Iodine contrast medium is injected in the vessels, which causes them to absorb more X-ray radiation than the surrounding tissues. (b) The vesselness transform of the X-ray image enhances the tubular structures, and suppresses the other image features.

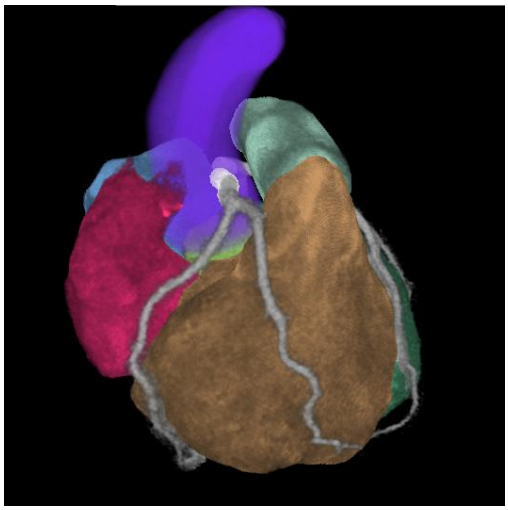

(a)

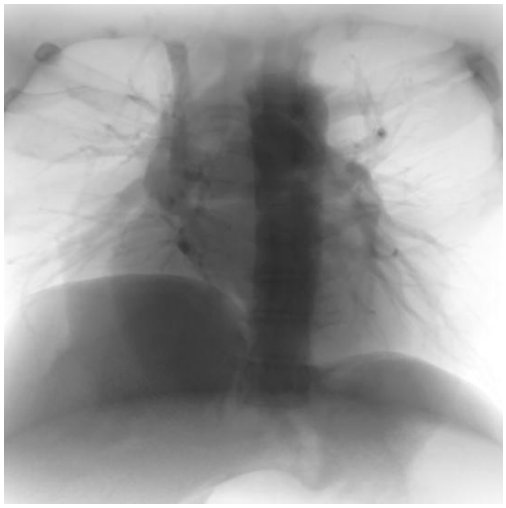

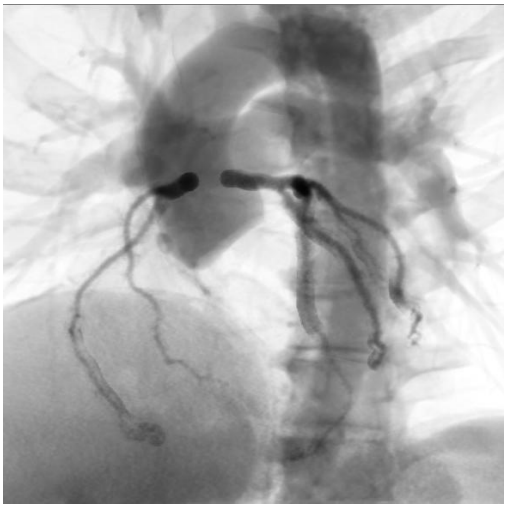

(b) (c)

Fig. 5. (a) Segmented cardiac CTA dataset. The gray tubular structures are the segmented coronary arteries. (b) A Digitally Reconstructed Radiograph (DRR) of the same dataset. Since the CTA is acquired with intravenously injected contrast agent, the cardiac atria and ventricles display more attenuation than in an X-ray angiogram. (c) A DRR, using different X-ray attenuation coefficients per segment, simulating X-ray angiography.

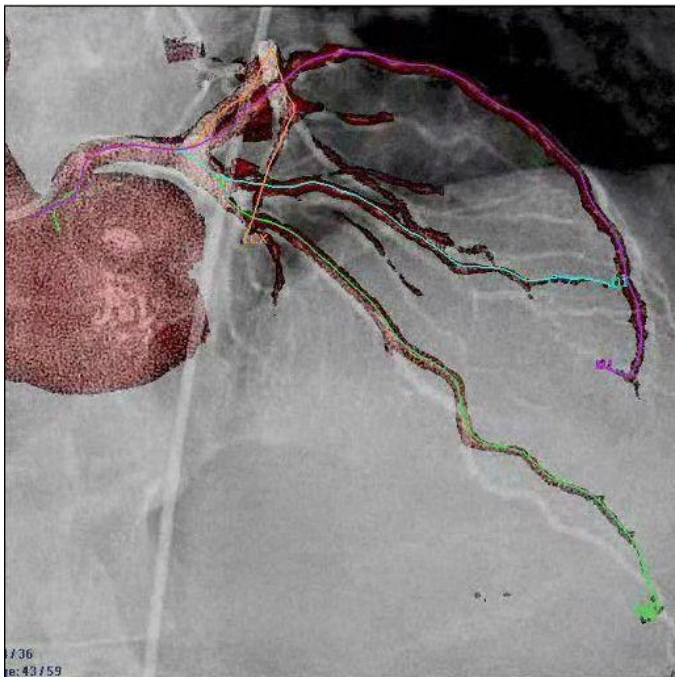

Fig. 6. A fused visualization of the coronary arteries, segment in a 3D CTA dataset (red), and 2D X-ray angiography image (gray). The combined visualization allows the correlation of the vessels in the CTA data (and pre-interventional annotations) and the peri-interventional X-ray by the observer.

Table 1. Average residual error (x) and stand deviation (σ) of a successful registration, measured using simulated data. The same set of initial transformations was used for all methods.

Similarity measure	ICP	Vesselness	Vesselness
Optimizer	Powell	Powell	Stochastic
Translation (mm)	$x = 1.44$, $\sigma = 1.50$	$x = 0.42$, $\sigma = 0.12$	$x = 0.54$, $\sigma = 0.47$
Rotation (degrees)	$x = 1.31°$, $\sigma = 1.00$	$x = 0.70°$, $\sigma = 0.77$	$x = 1.06°$, $\sigma = 1.00$

Table 2. The maximum capture range was established using clinical datasets.

Sim. meas.	ICP	ICP	Vesselness	Vesselness
Optimizer	Powell	Stochastic	Powell	Stochastic
Pair 1	0.0 mm, 0.0°	7.8 mm, 8.72°	83.3 mm, 21.7°	76.9 mm, 40.3°
Pair 2	21.8 mm, 17.5°	33.1 mm, 16.6°	68.7 mm, 31.9°	62.0 mm, 41.5°
Pair 3	12.9 mm, 25.2°	11.2 mm, 14.5°	49.7 mm, 23.8°	60.8 mm, 37.3°
Pair 4	12.1 mm, 11.0°	20.2 mm, 15.2°	30.8 mm, 30.3°	71.0 mm, 51.7°